Journal of Power Sources 486 (2021) 229371

Contents lists available at ScienceDirect

Journal of Power Sources

journal homepage: www.elsevier.com/locate/jpowsour

Stress evolution during the two-step charging of high-capacity electrode materials

Jiamei Guo, Zheng Jia *

Key Laboratory of Soft Machines and Smart Devices of Zhejiang Province, X-Mechanics Center, Department of Engineering Mechanics, Zhejiang University, Hangzhou, 310027, China

HIGHLIGHTS

- We develop a chemo-mechanical model for anodes undergoing the two-step charging.
- We reveal a unique stress mitigation mechanism inherent to the two-step charging.
- We study how nonlinear modulus-concentration relation affects stress evolution.

GRAPHICAL ABSTRACT

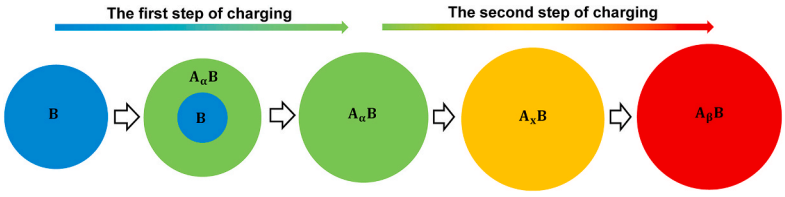

ARTICLE INFO

Keywords:
Two-step charging
Stresses
Finite element method
Young's modulus

ABSTRACT

It has been well recognized that the lithiation of crystalline silicon advances via a one-step two-phase mechanism. In stark contrast, other high-capacity anode materials including amorphous silicon, germanium, and tin for lithium-ion and sodium-ion batteries are charged through a two-step process. That is, the first step of charging advances by the movement of a reaction interface that separates a pristine phase and a partially charged phase until the pristine anode material is fully consumed. Then the second step of charging sets in without a visible interface, eventually resulting in the fully charged anode. Lithiation and associated stress generation in crystalline silicon have been extensively studied by experiments and simulations. However, little attention has been given to the charging mechanics of anodes undergoing two-step charging. In this work, by resorting to the finite element method, we develop a model to simulate the stress generation in nanoparticle anodes during the two-step charging process. The model accounts for the unique charge-carrier concentration profile during two-step charging and the elastic softening of anode materials. We find that these two factors, in concert, lead to effective stress mitigation during the second step of charging, yielding the tough charging behavior of anodes featuring the two-step charging mechanism.

1. Introduction

Lithium-ion batteries (LIBs) have become an indispensable source of energy for portable devices. Graphite is currently the state-of-the-art anode material for commercial lithium-ion batteries. Notably, the theoretical capacity of crystalline silicon (c-Si) reaches 4200 mA h/g, exceeding that of graphite (372 mA h/g) by almost 10 times [1,2]. In this regard, c-Si is emerging as a promising candidate material for anodes of lithium-ion batteries. However, despite the large capacity, c-Si has a major drawback – prone to fracture. The lithiation of c-Si anodes occurs via a two-phase mechanism, with a moving phase boundary separating a pristine c-Si core and a fully lithiated outer shell of $Li_{3.75}Si$ [3,4]. The

* Corresponding author.
E-mail address: zheng.jia@zju.edu.cn (Z. Jia).

https://doi.org/10.1016/j.jpowsour.2020.229371
Received 7 June 2020; Received in revised form 15 December 2020; Accepted 17 December 2020

drastic volume expansion (~280%) due to the insertion of lithium (Li) pushes out the $Li_{3.75}Si$ shell, causing excessive tensile stress in the surface layer of the anode. In addition, experimental evidence has accumulated that the lithiation of c-Si is highly anisotropic, featuring considerably large volume expansion along the <110> direction but negligibly small expansion along the <111> direction [5]. Such anisotropic expansion behavior induces significant stress concentration, further increasing the tensile stress level at specific sites of the particle surface. Consequently, driven by large hoop tension induced by the anisotropic two-phase lithiation, the fracture of c-Si anodes originates at the anode surface and occurs preferentially between adjacent <110> directions [4,6], pulverizing the c-Si anode structure and thereby undermining the cycling performance of the LIBs.

Motivated by the needs to mitigate mechanical degradation induced by anisotropic lithiation, c-Si has been designed into various nanostructures, such as nanofilms [7,8], nanowalls [9], nanowires [2,10,11], and nanoparticles [12–15]. Besides engineering the geometry of c-Si nanostructures, considerable efforts have been devoted to constructing lithium-ion batteries with alternative anode materials, such as amorphous silicon (a-Si), germanium (Ge), and tin (Sn). Insertion of lithium into a-Si induces a volume expansion of 280% at full charge, rendering the theoretical capacity of a-Si the same as that of c-Si (i.e., 4200 mA h/g). Notably, both experiments and simulations have revealed that lithiated a-Si anodes have a more gentle variation of Li profiles than c-Si anodes do, which endows a-Si with enhanced resistance to mechanical degradation [16–18]. Ge also has a high specific capacity, which is 1384 mA h/g for $Li_{15}Ge_4$ [19–21]. To achieve a high charging/discharging rate in LIBs, fast transport of both electrons and Li ions is highly desirable. The electronic conductivity and the lithium-ion diffusivity are higher in Ge than in Si [22,23], such that LIBs based on Ge anodes may possess better rate capacity and power density than Si-based LIBs. However, its low earth abundance and complicated processing technology make germanium an expensive material. Moreover, germanium has greater toxicity than materials such as tin. As another Group IV element, tin possesses a theoretical capacity of 994 mA h/g, about three times that of the commercialized graphite anode in current LIBs. Moreover, Sn is inexpensive, earth-abundant, and nontoxic, making it another promising candidate anode material for LIBs [24].

One salient feature of a-Si, Ge, and Sn anodes is the isotropic two-step lithiation process [18,19,25], which is in stark contrast to the anisotropic one-step lithiation that takes place in c-Si. In the first step, the lithiation occurs via a two-phase mechanism, with a migrating interface separating a pristine phase and an intermediate lithiated phase. Such an interface exists until the pristine phase is exhausted. Then the second step of lithiation advances via a one-phase mechanism without a visible interface, lithium concentration in the anodes ramps up continuously, ending up with fully lithiated anode materials. It has been revealed by experiments that the abovementioned anode materials undergoing two-step lithiation process are less susceptible to fracture than c-Si, as exemplified by their large critical fracture size below which anodes are immune to lithiation-induced fracture. Specifically, a-Si particles up to 870 nm in diameter do not fracture upon lithiation, and no cracking is observed after full lithiation in Ge spheres as large as 620 nm. These values are much larger than the 150 nm critical fracture diameter previously identified for c-Si particles. The tough mechanical behavior of a-Si, Ge, and Sn during lithiation is mainly ascribed to the more uniform and gentle stress profiles due to isotropic and two-step lithiation [17,18]. Although how isotropy in lithiation reaction alleviates stress concentration has been unveiled computationally [26], quantitative evidence corroborating the contribution of two-step lithiation is still lacking – the past decade has witnessed extensive studies on the stress generation in c-Si anode, but few efforts have been devoted to simulating stress evolution of anode materials subjected to two-step charging. In addition, the two-step charging process has not only been found in LIBs, but it also exists in battery systems beyond lithium chemistry, such as sodium(Na)-ion batteries (NIBs), and potassium (K)-ion batteries (KIBs) [25–27]. For instance, sodiation and potassiation of Sn anodes also take place via a two-step process [27,28]. However, the charging mechanics of electrodes in these novel batteries has garnered little attention. To this end, it is of practical significance to numerically study the stress generation of high-capacity electrode materials undergoing two-step charging. The results are expected to shed light on the understanding of the tough behavior of a-Si, Ge, and Sn anodes, and offer design guidelines for next-generation rechargeable batteries including LIBs, NIBs, and KIBs.

In this paper, by employing finite-element-based chemomechanical simulation, we report a systematic mechanistic study of the stress evolution in anodes subject to two-step charging. Our case studies on various anode systems, including Li/a-Si, Li/Ge, Li/Sn, and Na/Sn, reveal that the charging-induced elastic softening of anode materials leads to effective stress reduction during the second step of charging, giving rise to the tough mechanical behavior of anodes. That is, a unique stress mitigation mechanism that is inherent to the two-step charging process is identified. We demonstrate that the evolution of stress during two-step charging is strongly affected by two factors: the composition of the intermediate phase (namely, the concentration of guest atoms – Li, Na, and K – in the intermediate phase) and the variation of Young's modulus as charging proceeds. The mechanistic findings emerging from the present study can offer quantitative insights into the charging behavior of a myriad of high-capacity electrodes featuring the two-step charging mechanism. Since stress generation in electrodes during charging is critical to the performance of batteries, and little attention, if any, has been given to the stress generation in anodes featuring a two-step charging mechanism, the novelty and significance of the present study include. (i) We develop a first-of-its-kind mechanical model for studying stresses in anodes undergoing a two-step charging process. (ii) We identify a universal stress mitigation mechanism inherent to the two-step charging process, which explains the tough behavior of anodes featuring a two-step charging mechanism.

2. Computational model

Nanomaterials, especially nanoparticles, have been widely utilized as the basic building blocks to develop anodes for LIBs and NIBs, since the nanometer size scale shortens the diffusion path and reduces the driving force for crack formation, thereby enhancing both the rate capacity and resistance to mechanical failure of electrodes. For example, the pomegranate-inspired anode design that encapsulates individual silicon nanoparticles in carbon cages has been demonstrated with superior cyclability [14]. Understanding the stress evolution in an individual nanoparticle – the basic building block for various novel anodes – during charging lays the foundation for the development of next-generation high-performance batteries. For this reason, the computational model developed in the present work will focus on nanoparticle anodes that undergo two-step charging, as illustrated in Fig. 1(a).

2.1. Two-step charging

Fig. 1(a) sketches the two-step charging process during which guest atoms A (Li, Na, or K) are infiltrated into an anode particle of host material B (a-Si, Ge, or Sn). In the first step of charging, guest atoms migrate into the anode through the outer surface, forming an intermediate phase $A_\alpha B$ near the outer surface, which is separated by an atomically sharp interface from the pristine phase B. As charging goes on, the interface continuously moves, consuming the unreacted host material and leaving a thick $A_\alpha B$ shell in the wake of the moving interface, until the inner core of pristine phase B is completely consumed. The first step of charging ends up with a sphere of $A_\alpha B$. In this work, we examine the stress evolution in a-Si anodes, Sn anodes, and Ge anodes in LIBs, as well as Sn anodes in NIBs, for which the intermediate phase $A_\alpha B$ is $Li_{2.5}Si$, LiSn, $Li_{2.5}Ge$, and $Na_{0.5}Sn$, respectively (Table 1). In

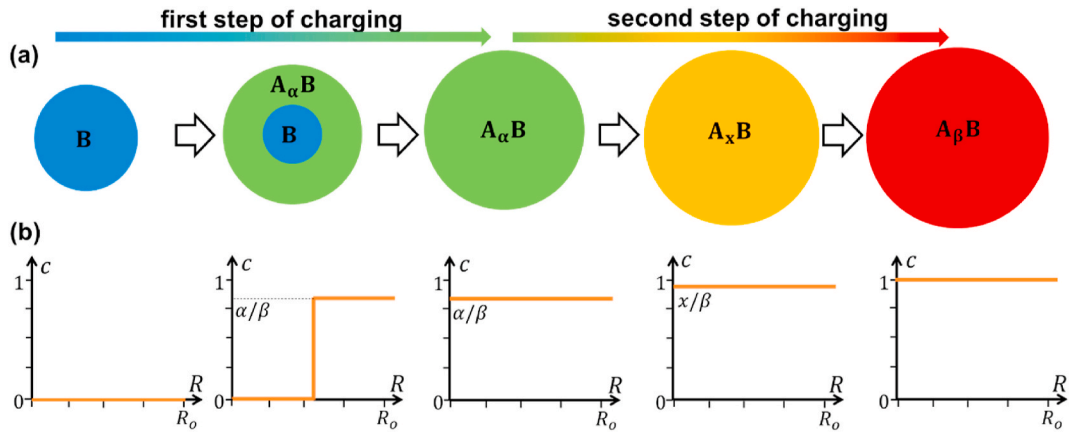

Fig. 1. Snapshots illustrating the two-step charging process and the corresponding distribution of guest atoms in the anodes. (a) In the first step, charging occurs via a two-phase mechanism with a reaction interface between pristine phase B and intermediate phase $A_\alpha B$ moving inwards until the phase B is exhausted, yielding a sphere of $A_\alpha B$ at the end of the first step. In the second step, the intermediate phase $A_\alpha B$ evolves into $A_\beta B$ without a visible interface. (b) The profile of normalized concentration of guest atom A in anodes as charging advances. R_o is the outer radius of the nanoparticle in its undeformed configuration.

Table 1
The volume expansion ratio, the composition of the intermediate phase, and the composition of the fully-charged phase of the four anode systems studied.

The anode system	The volume expansion ratio **η**	The intermediate phase ($\mathbf{A_\alpha B}$)	The fully-charged phase ($\mathbf{A_\beta B}$)
Li/Ge [19]	246%	$Li_{2.5}Ge$	$Li_{3.75}Ge$
Li/Sn [25]	258%	LiSn	$Li_{4.4}Sn$
Li/a-Si [18]	280%	$Li_{2.5}Si$	$Li_{3.75}Si$
Na/Sn [27]	420%	$Na_{0.5}Sn$	$Na_{3.75}Sn$

the second step, the anode is charged from the intermediate phase $A_\alpha B$ to the fully charged phase $A_\beta B$ via a single-phase mechanism without an interface. The final product, $A_\beta B$, is $Li_{3.75}Si$, $Li_{4.4}Sn$, $Li_{3.75}Ge$, and $Na_{3.75}Sn$ for the Li/a-Si, Li/Sn, Li/Ge, and Na/Sn system, respectively (Table 1). To visualize the distribution of A in the anodes during the two-step charging process, we plot the normalized concentration c of guest atom A in Fig. 1(b), which is defined as the current concentration of A divided by the concentration in the fully charged state. For example, denote the current phase by A_xB ($0 \le x \le \beta$), the normalized concentration c is given by x/β. Note that R_o is the outer radius of the nanoparticle in its undeformed configuration.

We study the two-step charging process and the concurrent stress generation by employing the commercialized finite element package ABAQUS. The phase evolution as well as the migration of the interface during the two-step charging is modeled by a nonlinear diffusion model, with the conductivity given by

$$D = \begin{cases} D_0[1/(c_I - c) - 2c] & \text{if } c < c_I \text{ and } D \le 10^3 D_0 \\ 10^3 D_0 & \text{otherwise} \end{cases} \quad (1)$$

where D_0 is a model constant, c_I represents the normalized concentration of guest atom A in the intermediate phase, which is defined as α/β. To simulate the first step of charging, we set the boundary condition $c(R_o) = c_I$ at the surface of the particle. The diffusivity given in Eq. (1) is considerably large in the $A_\alpha B$ shell and is negligibly small in the unreacted core, such that the normalized concentration of guest atoms in the wake of the migrating interface can quickly attain the value $c = c_I$, while that ahead of the front remains zero. This produces a moving interface in the first step of charging, as observed in experiments [18,27]. In the second step, the anode particle is subjected to a constant flux at the surface; the fast diffusion of guest atoms driven by the diffusivity of $10^3 D_0$ gives a gentle variation of concentration profiles. The above nonlinear diffusion model is implemented as a user material subroutine for heat transfer (UMATHT) to interface with ABAQUS, updating diffusivities based on the current concentration c. D_0 is set to be 10^{-17} m^2/s. Although voltage profiles are not used in the modeling, it is still important to mention how voltage profile evolves during two-step charging under galvanostatic conditions: (i) During the first step of charging, the voltage remains a constant since the charging process is reaction-controlled. (ii) During the second step of charging, the voltage decreases with time, because the charging process is diffusion-controlled [29].

2.2. Charging-induced volume expansion

During charging, guest atoms A are infiltrated into the anodes and alloy with the host material B, eventually forming the final product $A_\beta B$ and causing drastic volume expansion of the anodes. For example, a-Si anodes in LIBs are lithiated to $Li_{3.75}Si$ upon full charging, resulting in a volume expansion of 280% (Table 1). In the following, we use η to denote the ratio of the volume of the fully charged phase ($A_\beta B$) over the volume of the pristine anode material (B), such that η for the Li/a-Si system is 3.8. Charging-induced volume expansion for various anode materials has been observed and measured experimentally [18,25–27]. Based on data in the literature, the volume expansion ratio η for Li/Sn, Li/Ge, and Na/Sn systems is 3.58, 3.46, and 5.2, respectively (Table 1).

In the modeling, the volumetric strain caused by the insertion of guest atoms is proportional to the normalized concentration c, i.e., $\varepsilon_{ij}^v = \tau\delta_{ij}c$ $(i,j = 1, 2, 3)$, where ε_{ij}^v is the charging-induced volumetric strain, δ_{ij} is the Kronecker delta, and τ is the charging-induced volume expansion coefficient. When the anode material is fully charged, the normalized concentration of the guest atoms reaches unity, namely, $c = 1$, and thus the volumetric strains at full capacity are given by $\varepsilon_{11}^v = \varepsilon_{22}^v = \varepsilon_{33}^v = \tau$. In ABAQUS, ε_{ij}^v represents true strain defined on the deformed configuration, such that the corresponding stretch ratio is $\lambda_{11}^v = \lambda_{22}^v = \lambda_{33}^v = e^\tau$, giving rise to the volume expansion ratio $\eta = \lambda_{11}^v\lambda_{22}^v\lambda_{33}^v = e^{3\tau}$. To this end, the charging-induced volume expansion coefficient τ is related to the volume expansion ratio η by

$$\tau = \frac{1}{3}\ln\eta \quad (2)$$

According to Eq. (2), for Li/a-Si, Li/Sn, Li/Ge, and Na/Sn anode systems, τ equals to 0.445, 0.425, 0.414, and 0.550, respectively. These values of τ are assigned to ABAQUS in order to simulate the large volume expansion caused by charging. The NLGEOM option in ABAQUS is switched on to account for large nonlinear geometrical changes induced by charging.

2.3. Concentration-dependent mechanical properties

First-principles calculations have revealed that Young's modulus and Poisson's ratio of lithiated and sodiated anode materials both decrease as charging advances [30]. It has been widely recognized that the insertion of guest atoms (e.g., lithium) facilitates the breaking of bonds in host materials (e.g., Si–Si bond in a-Si anodes) and formation of weaker bonds between guest and host atoms (e.g., Li–Si bond in Li/a-Si system) [30,31]. This results in a reduction in Young's modulus with increasing concentration of guest atoms, a phenomenon widely referred to as the elastic softening [32,33]. We summarize the concentration-dependent mechanical properties of Li/Ge, Li/Sn, Li/a-Si, and Na/Sn anode systems in Table 2. For Ge anodes in Li-ion batteries, Young's modulus and Poisson's ratio of pristine Ge are 102.7 GPa and 0.28, respectively [34]. During lithiation, Ge anodes undergo drastic elastic softening, with Young's modulus eventually reducing to 46.7 GPa and Poisson's ratio diminishing to 0.22 at full lithiation ($Li_{3.75}Ge$) [35]. Sn can act as the anode material for both LIBs and NIBs, possessing Young's modulus of 51 GPa and a Poisson's ratio of 0.34 [24]. In LIBs, the full lithiation of Sn anode results in a final product of $Li_{4.4}Sn$, with a significantly lower Young's modulus of 24.7 GPa and a Poisson's ratio of 0.24 [24]; In NIBs, $Na_{3.75}Sn$ is formed at full charging of which Young's modulus and Poisson's ratio become 15 GPa and 0.31, respectively [33]. Elastic softening has also been observed in a-Si anodes under lithiation, Young's modulus and Poisson's ratio of a-Si diminish with increasing Li concentration from 96 GPa to 0.28 for pristine a-Si to 41 GPa and 0.25 for $Li_{3.75}Si$ [24]. As to be shown later, such charging-induced elastic softening plays a pivotal role in affecting the stress evolution of high-capacity anodes undergoing two-step charging. In the finite element modeling, mechanical properties of pristine anode materials ($c = 0$) and fully charged anode materials ($c = 1$) are adopted from Table 2; We assume that both Young's modulus and Poisson's ratio of the anode materials vary linearly with the concentration of guest atoms. Moreover, experiments have indicated that Si and Ge anodes deform plastically when the stress exceeds the yield strength during lithiation [36,37]. The plastic deformation is engendered by the repeated breaking and re-forming of Si–Si bonds and Li–Si bonds [30,31]. It is reasonable to surmise that other anode materials undergoing two-step charging also experience plastic deformation because of the continuous bond breaking and formation facilitated by the insertion of guest atoms. In simulations, the yield strength σ_Y of the charged anode material is taken to be $0.01E_B$, where E_B denotes Young's modulus of the pristine anode material B.

3. Results and discussion

3.1. Stress evolution and mitigation during two-step charging

To show the stress distribution and evolution during two-step charging, we take a Ge nanoparticle anode in LIBs as an example. As mentioned earlier, the lithiation of Ge advances via a two-step process [19]: The first step is marked by a moving interface that separates the pristine Ge ($c = 0$) ahead of the interface and the $Li_{2.5}Ge$ intermediate phase ($c = 0.67$) in the wake (see the inset of Fig. 2(a)). In the second step, the anode is gradually lithiated from the $Li_{2.5}Ge$ intermediate phase ($c = 0.67$) to the $Li_{3.75}Ge$ phase ($c = 1$), as illustrated by the insets of Fig. 2(b)–(d).

Fig. 2(a)–(d) plots the distribution and contours of three stress components – including von Mises stress σ_{mises}, hoop stress σ_θ, and radial stress σ_r, all normalized by the yield strength σ_Y – at four representative stages. In the first step of lithiation, as shown in Fig. 2(a), the inner unlithiated core of the Ge particle is under hydrostatic stress state with $\sigma_r = \sigma_\theta$, resulting in zero von Mises stress. In the vicinity of the interface, the constraint from the inner unlithiated core acts against the volume expansion of the outer $Li_{2.5}Ge$ shell. Hence, the $Li_{2.5}Ge$ phase near the interface is under compressive hoop stress, and the resulting von Mises stress readily reaches the yield strength, causing plastic deformation in the $Li_{2.5}Ge$ shell. As the interface moves inwards, more anode materials in the wake of the interface are lithiated and expand in volume, pushing out $Li_{2.5}Ge$ shell near the outer surface and stretching the shell in the hoop direction. In consequence, the hoop stress σ_θ in the $Li_{2.5}Ge$ shell near the particle surface becomes tensile and reaches σ_Y in the surface layer. The stress distribution in the Ge particle during the first step of lithiation is very much like that in a lithiated c-Si particle [38], since in both cases the lithiation is dominated by a two-phase lithiation mechanism. At the end of the first step, the anode particle experiences a high level of stresses. As seen from Fig. 2(b), the tensile hoop stress at the particle surface remains to be σ_Y and almost the entire anode attains plastic yielding with the von Mises stress being σ_Y.

In the second step of lithiation, the most salient feature is the stress reduction. Fig. 2(b)–(d) show that magnitudes of hoop stress, radial stress, and von Mises stress decrease as charging continues. The stress reduction is attributed to both the elastic softening discussed in Section 2.3 and the gentle Li profile in the second step of charging mentioned in Section 2.1. More details of the mechanism underpinning the stress reduction will be discussed later in Sec. 3.3. In particular, results in Fig. 2(b)–(d) indicate that the tensile hoop stress σ_θ at the particle surface ($R/R_o = 1$) decreases from σ_Y at the end of the first step (Fig. 2(a)), to $0.79\sigma_Y$ when the particle is lithiated to Li_3Ge (Fig. 2(c)), and eventually to $0.66\sigma_Y$ in the fully lithiated particle (Fig. 2(d)). Since high tensile hoop stress at the outer surface may consequently trigger the fracture of the anode particle [16,39–42], the drop in magnitude of the hoop tensile stress can effectively mitigate the charging-induced fracture, thereby imparting tough lithiation behavior to Ge anodes. It is worth noting that the stress generation and evolution in Li/a-Si, Li/Sn, and Na/Sn anode systems are similar to that of Ge anodes in LIBs shown in Fig. 2. A common feature of the stress evolution in anodes undergoing two-step charging is the significant stress reduction that takes place in the second step of charging. In sharp contrast, although insertion of lithium also cause elastic softening of c-Si, the lithiation of c-Si takes a one-step process and consequently the stress level remains considerably high during the entire charging, rendering c-Si prone to charging-induced fracture [38].

3.2. Hoop stress in the surface layer in various anode systems

As mentioned earlier, the magnitude of hoop stress in the surface layer of anode particles plays a critical role in dictating the fracture behavior of anodes. In Fig. 3, we plot the normalized hoop stress in the surface layer (namely, hoop stress divided by the yield strength of the materials) as a function of the state of charge (SOC) for all anode systems studied in this work. The SOC can be evaluated by $SOC = 3R_o^{-3}\int_0^{R_o} c(R)R^2dR$, where R_o is the outer radius of the particle in the initial configuration, radius R represents the position of a material element and $c(R)$ is the normalized concentration at radius R. Note that SOC = 0 represents the uncharged state of the anode, and SOC = 1 the fully-charged state. For the Ge anode in the LIBs, as lithiation starts, the

Table 2
Young's modulus and Poisson's ratio of pristine and fully-charged anode materials.

Anode System	Young's Modulus (GPa)	Poisson's Ratio	Phase
Li/Ge [34,35]	102.7	0.28	Ge
	46.7	0.22	$Li_{3.75}Ge$
Li/Sn [24]	51.0	0.34	Sn
	24.7	0.24	$Li_{4.4}Sn$
Li/a-Si [24]	96.0	0.29	a-Si
	41.0	0.25	$Li_{3.75}Si$
Na/Sn [33]	51.0	0.34	Sn
	15.0	0.31	$Na_{3.75}Sn$

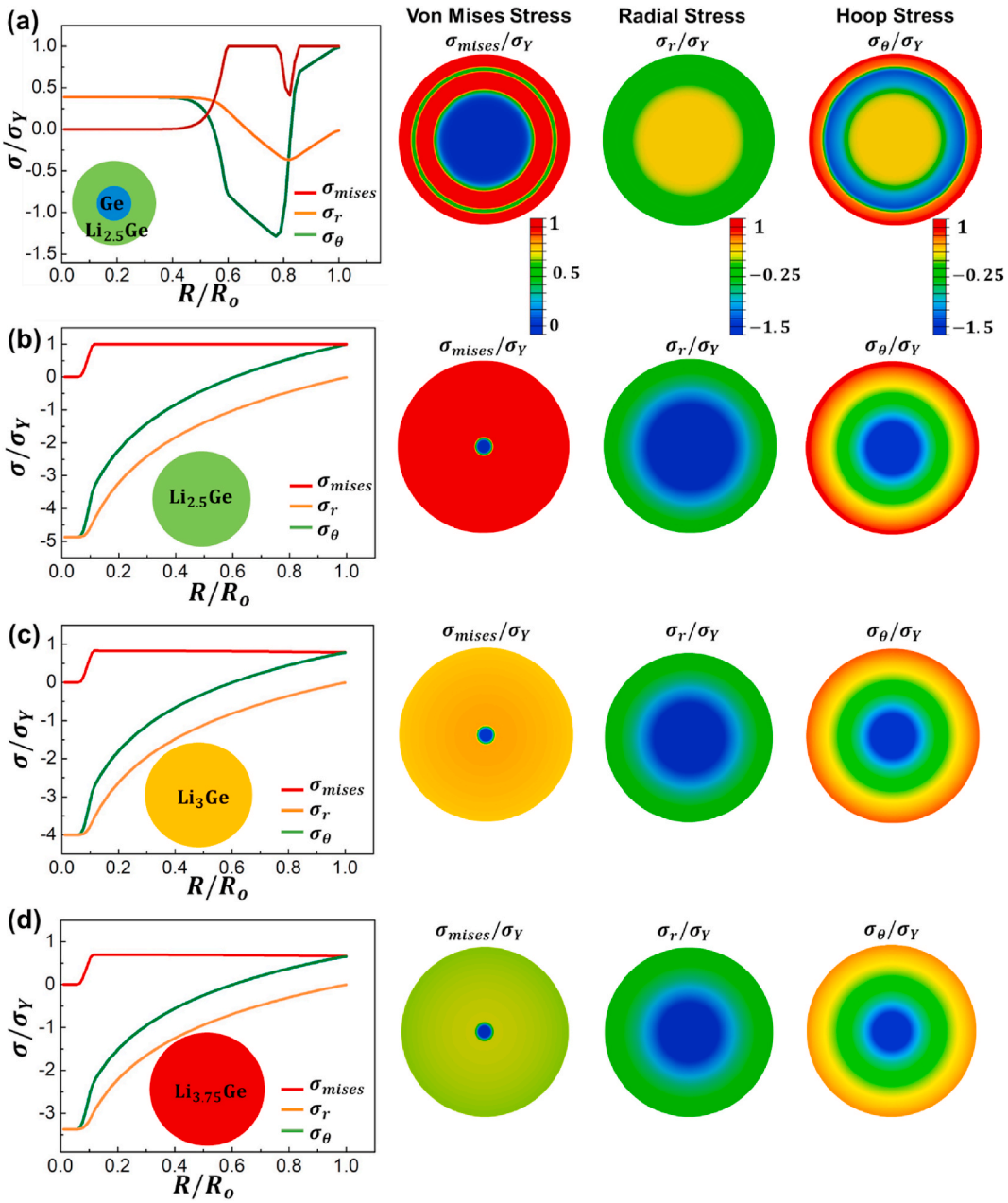

Fig. 2. Evolution of stresses in a Ge nanoparticle during two-step charging. (a) and (b) show the distribution of stress components in the first step of charging; (c) and (d) demonstrate the stress profiles in the second step. Insets in (a–d) show the stages of charge. Corresponding stress contours are also presented. From left to right, the three columns represent the distribution of von Mises stress, radial stress, and hoop stress, respectively.

insertion of lithium atoms causes the surface layer of the particle to swell. The constraint from the inner unlithiated core acts against the volume expansion and generates significant compressive stress in the surface layer, leading to compressive plastic yielding with $\sigma_\theta(R_O) = -\sigma_Y$. As the interface moves forward, lithiation-induced swelling of materials right behind the interface pushes out the $Li_{2.5}Ge$ shell behind the migrating interface, thereby stretching the surface layer in the hoop direction and reversing the initial compressive plastic yielding into tensile yielding with $\sigma_\theta(R_O) = \sigma_Y$. The tensile plastic yielding maintains until the SOC reaches 0.67, which marks the end of the first step of lithiation. In the second step of charging, the SOC ramps up from 0.67 to 1, and the hoop stress at the surface layer decreases linearly from σ_Y to $0.66\sigma_Y$. As discussed above, the mechanism of this stress drop is due to a combined effect of the two-step charging process and the elastic softening. In Fig. 3, it is further noted that the $\sigma_\theta(R_O)$ curve of a-Si anodes almost coincides with that of the Ge anode, ending up with $\sigma_\theta(R_O) = 0.64\sigma_Y$. For Li–Sn and Na–Sn anode systems, the intermediate phases are LiSn and $Na_{0.5}Sn$, respectively, and the corresponding SOC at the end of the first-step charging is 0.23 and 0.13. After the second step of charging, the hoop stress in the surface layer of $Li_{4.4}Sn$ becomes $0.45\sigma_Y$, and that in $Na_{3.75}Sn$ reduces to $0.28\sigma_Y$, both of which are lower than that in Ge and a-Si anodes.

3.3. Theoretical analysis

Secs. 3.1 and 3.2 have investigated the stress evolution of various anode systems that undergo the two-step charging process. Results indicate that the first step of charging leads to the buildup of high stresses, while the second step yields a continuous drop in the stress level. Nevertheless, a key question remains unclear: what is the mech-

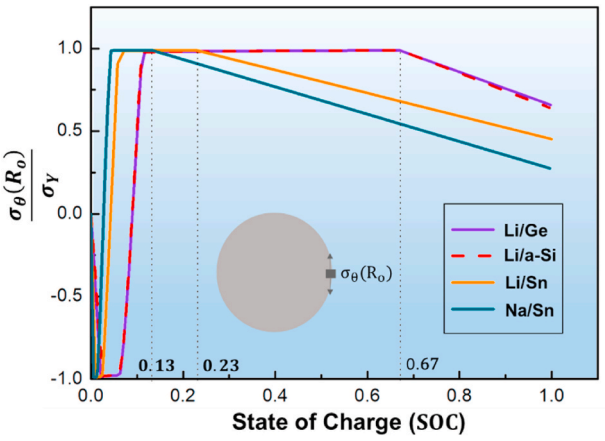

Fig. 3. The evolution of hoop stress at the particle surface in various anodes undergoing two-step lithiation process.

anism underpinning the stress reduction occurring in the second step of charging? As an effort to find the answer to the above question and validate the simulation results presented in previous sections, we next outline a simple theoretical model to determine the hoop stress in the surface layer after full charging, and compare the theoretical predictions to modeling results given in Fig. 3. It has been noted in several theoretical studies that two-phase charging mechanism, like the lithiation of c-Si or the first-step of charging in Ge anodes, leads to tensile plastic yielding in the surface layer of anode particles so that the surface hoop stress $\sigma_\theta(R_O)$ equals to σ_Y [16,38,43]. During the second step of charging, the variation of the concentration of guest atoms in the anode is gentle [18,19]. Therefore, the anode swells uniformly during the second step, hardly changing the elastic and plastic strain fields. Moreover, as aforementioned, the Young's modulus of the current phase A_xB decreases from $E_{A_\alpha B}$ to $E_{A_\beta B}$ in the second step, where $E_{A_\alpha B}$ and $E_{A_\beta B}$ represent the Young's modulus of the intermediate phase and that of the final product, respectively. Such elastic softening as well as the almost unchanged strain fields causes elastic unloading and reduces the stress level to the elastic regime. For simplification, we assume the elastic and plastic strains remain fixed during the second step of charging and ignore the variation of Poisson's ratio during charging. Then it arrives that the surface hoop stress at the end of charging is proportional to that at the end of the first step in a fashion that $\sigma_\theta(R_O) = \frac{E_{A_\beta B}}{E_{A_\alpha B}}\sigma_Y$, at SOC = 1. Moreover, it has been assumed that the Young's modulus of A_xB linearly decreases as the value of x increases, that is, the Young's modulus of the intermediate phase $E_{A_\alpha B}$ can be given by $E_{A_\alpha B} = E_B - (E_B - E_{A_\beta B})\frac{\alpha}{\beta}$. Then we obtain that, at the end of charging,

$$\frac{\sigma_\theta(R_O)}{\sigma_Y} = \left[\frac{E_B}{E_{A_\beta B}} - \left(\frac{E_B}{E_{A_\beta B}} - 1\right)\frac{\alpha}{\beta}\right]^{-1} \quad (3)$$

Given an anode system, surface hoop stress at the end of charging can be evaluated by using Eq. (3). For instance, for Ge anodes in Li-ion batteries, $E_B = 102.7$ GPa, $E_{A_\beta B} = 46.7$ GPa, $\alpha = 2.5$, and $\beta = 3.75$, plugging these values into Eq. (3) gives $\frac{\sigma_\theta(R_O)}{\sigma_Y} = 0.71$. In this way, surface hoop stress at the end of charging in Li/a-Si, Li/Sn, and Na/Sn anode systems are evaluated to be 0.69, 0.55, and 0.32, respectively. Notably, the theoretical predictions agree reasonably well with the results from finite element simulations – 0.71 vs. 0.66 for Li/Ge, 0.69 vs. 0.64 for Li/a-Si, 0.32 vs. 0.28 for Na/Sn – considering that the theoretical analysis invokes various simplified assumptions such as constant Poisson's ratio. However, the Poisson's ratio of Sn anodes decreases considerably from 0.34 to 0.24 during lithiation, such that the theoretical analysis suggests $\frac{\sigma_\theta(R_O)}{\sigma_Y} = 0.55$ while the finite element modeling gives 0.45.

3.4. Linear vs. nonlinear variation of Young's modulus

As discussed earlier, when guest atoms (e.g. Li and Na) are continuously inserted into anodes, Young's modulus of the charged phase diminishes with increasing concentration of guest atoms. Previous studies [16], including simulation results presented in Sec. 3.1-3.3 of this work, assume that Young's modulus changes linearly as the concentration of guest atoms increases for simplification. However, Ab initio calculations have indicated that the dependence of Young's modulus of lithiated silicon on the Li concentration is not necessarily linear [30]. To explore the influence of the nonlinear variation of modulus with increasing concentration of guest atoms, we take Ge anodes as an example, examining the stress evolution when the modulus of lithiated Ge decreases in a nonlinear fashion as Li concentration increases. Fig. 4(a) shows the comparison between the linear modulus-concentration relation adopted in Sec. 3.1-3.3 and three nonlinear cases; Evolution of Young's modulus in all three nonlinear cases starts at 102.7 GPa for $c = 0$, and continuously descents to 46.7 GPa at $c = 1$ following a nonlinear path which is convex downward. Fig. 4(b) shows the surface hoop stress as well as the stress contours at the end of charging for the four cases. One notes that the case #4 of the linear modulus-concentration relation yields the lowest surface hoop stress at the end of charging. As analyzed in Sec. 3.3, the surface hoop stress at the end of charging can be approximated by $\frac{E_{Li_{3.75}Ge}}{E_{Li_{2.5}Ge}}\sigma_Y$. Evidently, given that $E_{Li_{3.75}Ge} = 46.7$ GPa, the larger the value of $E_{Li_{2.5}Ge}$ is, the smaller the surface hoop stress at the end of charging. Therefore, Ge anodes with a linear modulus-concentration dependence experience the lowest surface tension after being fully charged. The above results reveal that dependence of Young's modulus on the concentration of guest atoms plays a nontrivial role in affecting stress evolution of anodes under two-step charging. Assuming a linear modulus-concentration relation may lead to underestimation of the stress generated during the second step of charging.

4. Discussions

It is worth noting that the two-step or two-phase charging not only takes place in electrode materials mentioned above but also in some transition metal oxides such as NiO and CuO [44]. Electrode materials in lithium-ion batteries can be classified into two categories: (1) intercalation-type materials, (2) alloying and conversion-type materials, based on the lithium storage mechanism. Conventional electrode materials (e.g. graphite) host lithium ions via physical intercalation, which involves insertion and removal of lithium ions within the lattice structure of the electrode materials, without chemically forming any new phases. Volumetric changes of intercalation-type electrodes during cycling are often small (~5%–10%). Moreover, the variation of lithium concentration within the electrodes is smooth and gentle, since the lithiation process is one-step one-phase. Therefore, lithiation-induced stresses in intercalation-type electrodes are moderate. In stark contrast, alloying and conversion-type materials react with lithium ions, which is characterized by the formation of entirely new phases and considerable volume change (100%–300%). Typical alloying and conversion-type materials include Si, Sn, Ge discussed above and transition metal oxides such as NiO, and CuO. In general, these alloying and conversion-type electrode materials often undergo a two-step two-phase charging process involving the growth of a new lithiated phase. Due to the pushing-out effect caused by the large volume expansion of the electrode particles, the hoop stress on the outer surface of the particle is large, leading to radial crack formation. One notes that transition metal oxides have garnered much attention due to their high theoretical capacity. For example, NiO has been demonstrated as a high areal capacity electrode in flexible lithium-ion batteries, with excellent cyclic stability and attractive rate capacity [45,46]. However, stress generation in transition metal oxides during charging remains largely unexplored. We

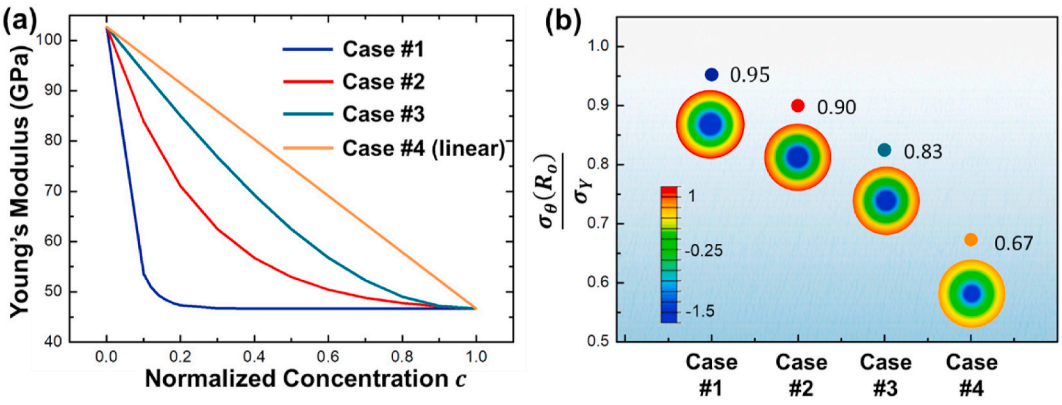

Fig. 4. (a) Concentration-dependent Young's modulus of Ge anodes. (b) The corresponding surface hoop stress at the end of charging. The color contours show the distribution of hoop stress after the anode is fully charged. (For interpretation of the references to color in this figure legend, the reader is referred to the Web version of this article.)

would like to point out that the mechanical model for the two-step charging developed in this paper can be applied to understand the lithiation process of transition metal oxides.

5. Conclusions

This work studies the stress generation in anodes undergoing two-step charging by resorting to finite element modeling. Anodes investigated include a-Si anodes, Ge anodes, and Sn anodes in lithium-ion batteries, and Sn anodes in sodium-ion batteries. The model accounts for the evolution of concentration profiles of guest atoms during the two-step charging process, as well as the large volume change and elastic softening caused by charging. It is revealed that the existence of a moving interface during the first-step of charging generates high tensile stress in the surface layer of particle anodes, while the second step of charging gives rise to a stress drop, reducing the mechanical driving force for crack formation and thus enhancing the resistance to mechanical failure. The stress relaxation can be ascribed to two factors: the gentle variation of guest atom concentration in anodes during the second step of charging, and the elastic softening. Among all the anodes studied in this work, the Sn anodes in sodium-ion batteries undergo the lowest stresses at the end of charging. To understand the mechanism of stress reduction and validate the simulation results, we further outline a simple theoretical model to evaluate the tensile stress in the surface layer of anode after full charging; Tensile hoop stresses obtained from the theoretical analysis agree quantitatively with the results of finite element modeling. Both the finite element modeling and theoretical analysis underscore the importance of the composition of the intermediate phase in dictating the charging-induced stresses: the fewer guest atoms the intermediate phase contains, the stiffer the intermediate phase is, and the lower the stresses are at the end of charging. Finally, we also examine the assumption of linear modulus-concentration relation widely adopted in related studies, since first-principles calculations suggest the dependence of modulus on concentration is not linear. The results imply that assuming the linear modulus-concentration relation may underestimate the stresses in the second step of charging. Ultimately, our findings shed fundamental insight into quantitative understanding about stress generation and evolution in anodes undergoing two-step charging, which holds the key to the control and mitigation of charging-induced fracture.

CRediT authorship contribution statement

Jiamei Guo: Formal analysis, Investigation, Writing - original draft. **Zheng Jia:** Conceptualization, Methodology, Supervision, Writing - review & editing.

Declaration of competing interest

The authors declare that they have no known competing financial interests or personal relationships that could have appeared to influence the work reported in this paper.

Acknowledgments

This work is supported by the National Natural Science Foundation of China through a grant on lithium-ion batteries (Grant number: 11802269). Zheng Jia also acknowledges the financial support from the One-Hundred Talents Program of Zhejiang University.

References

[1] J. Li, J.R. Dahn, J. Electrochem. Soc. 154 (2007) A156–A161.
[2] C.K. Chan, H. Peng, G. Liu, K. McIlwrath, X.F. Zhang, R.A. Huggins, Y. Cui, Nat. Nanotechnol. 3 (2008) 31–35.
[3] F. Fan, H. Yang, Z. Zeng, Scripta Mater. 152 (2018) 74–78.
[4] X.H. Liu, H. Zheng, L. Zhong, S. Huan, K. Karki, L.Q. Zhang, Y. Liu, A. Kushima, W. T. Liang, J.W. Wang, J.H. Cho, E. Epstein, S.A. Dayeh, S.T. Picraux, T. Zhu, J. Li, J. P. Sullivan, J. Cumings, C. Wang, S.X. Mao, Z.Z. Ye, S. Zhang, J.Y. Huang, Nano Lett. 11 (2011) 3312–3318.
[5] H. Yang, S. Huang, X. Huang, F. Fan, W. Liang, X.H. Liu, L.Q. Chen, J.Y. Huang, J. Li, T. Zhu, S. Zhang, Nano Lett. 12 (2012) 1953–1958.
[6] S.W. Lee, M.T. McDowell, L.A. Berla, W.D. Nix, Y. Cui, Proc. Natl. Acad. Sci. U.S.A. 109 (2012) 4080–4085.
[7] L. Yang, H.S. Chen, H. Jiang, Y.J. Wei, W.L. Song, D.N. Fang, Chem. Commun. 54 (2018) 3997–4000.
[8] J. Chen, L. Yang, Y. Han, Y.H. Bao, K.L. Zhang, X. Li, J. Pang, H.S. Chen, W.L. Song, Y.J. Wei, J. Power Sources 444 (2019), 227227.
[9] J. Wan, A.F. Kaplan, J. Zheng, X. Han, Y. Chen, N.J. Weadock, N. Faenza, S. Lacey, T. Li, J. Guo, L. Hu, J. Mater. Chem. 2 (2014) 6051–6057.
[10] T.D. Bogart, D. Oka, X. Lu, M. Gu, C. Wang, B.A. Korgel, ACS Nano 8 (2014) 915–922.
[11] S.W. Lee, H.W. Lee, I. Ryu, W.D. Nix, H. Gao, Y. Cui, Nat. Commun. 6 (2015).
[12] R. Xu, K. Zhao, Extreme Mechanics Letters 8 (2016) 13–21.
[13] Z. Chen, C. Wang, J. Lopez, Z. Lu, Y. Cui, Z. Bao, Advanced Energy Materials 5 (2015).
[14] N. Liu, Z. Lu, J. Zhao, M.T. McDowell, H.W. Lee, W. Zhao, Y. Cui, Nat. Nanotechnol. 9 (2014) 187–192.
[15] B. Liu, Y. Jia, J. Li, H. Jiang, S. Yin, J. Xu, J. Power Sources (2020) 450.
[16] Z. Jia, T. Li, J. Mech. Phys. Solid. 91 (2016) 278–290.
[17] M.T. McDowell, S.W. Lee, J.T. Harris, B.A. Korgel, C. Wang, W.D. Nix, Y. Cui, Nano Lett. 13 (2013) 758–764.
[18] J.W. Wang, Y. He, F. Fan, X.H. Liu, S. Xia, Y. Liu, C.T. Harris, H. Li, J.Y. Huang, S. X. Mao, T. Zhu, Nano Lett. 13 (2013) 709–715.
[19] Y. Liu, S. Zhang, T. Zhu, Chemelectrochem 1 (2014) 706–713.
[20] D. Larcher, S. Beattie, M. Morcrette, K. Edstroem, J.C. Jumas, J.M. Tarascon, J. Mater. Chem. 17 (2007) 3759–3772.
[21] L. Baggetto, P.H.L. Notten, J. Electrochem. Soc. 156 (2009) A169–A175.
[22] J. Graetz, C.C. Ahn, R. Yazami, B. Fultz, J. Electrochem. Soc. 151 (2004) A698–A702.
[23] C.K. Chan, X.F. Zhang, Y. Cui, Nano Lett. 8 (2008) 307–309.
[24] Y. Qi, L.G. Hector Jr., C. James, K.J. Kim, J. Electrochem. Soc. 161 (2014) F3010–F3018.

[25] J. Wang, F. Fan, Y. Liu, K.L. Jungjohann, S.W. Lee, S.X. Mao, X. Liu, T. Zhu, J. Electrochem. Soc. 161 (2014) F3019–F3024.
[26] W. Liang, H. Yang, F. Fan, Y. Liu, X.H. Liu, J.Y. Huang, T. Zhu, S. Zhang, ACS Nano 7 (2013) 3427–3433.
[27] J.W. Wang, X.H. Liu, S.X. Mao, J.Y. Huang, Nano Lett. 12 (2012) 5897–5902.
[28] Q. Wang, X. Zhao, C. Ni, H. Tian, J. Li, Z. Zhang, S.X. Mao, J. Wang, Y. Xu, J. Phys. Chem. C 121 (2017) 12652–12657.
[29] M. Pharr, K. Zhao, X. Wang, Z. Suo, J.J. Vlassak, Nano Lett. 12 (2012) 5039–5047.
[30] K. Zhao, W.L. Wang, J. Gregoire, M. Pharr, Z. Suo, J.J. Vlassak, E. Kaxiras, Nano Lett. 11 (2011) 2962–2967.
[31] F. Fan, S. Huang, H. Yang, M. Raju, D. Datta, V.B. Shenoy, A.C.T. van Duin, S. Zhang, T. Zhu, Model. Simulat. Mater. Sci. Eng. (2013) 21.
[32] V.B. Shenoy, P. Johari, Y. Qi, J. Power Sources 195 (2010) 6825–6830.
[33] M. Mortazavi, J. Deng, V.B. Shenoy, N.V. Medhekar, J. Power Sources 225 (2013) 207–214.
[34] J.J. Wortman, R.A. Evans, J. Appl. Phys. 36 (1965) 153–156.
[35] R. Gaillac, P. Pullumbi, F.X. Coudert, J. Phys.: Condens. Matter 28 (2016) 275201.
[36] M.J. Chon, V.A. Sethuraman, A. McCormick, V. Srinivasan, P.R. Guduru, Phys. Rev. Lett. 107 (2011).
[37] M. Pharr, Y.S. Choi, D. Lee, K.H. Oh, J.J. Vlassak, J. Power Sources 304 (2016) 164–169.
[38] S. Huang, F. Fan, J. Li, S. Zhang, T. Zhu, Acta Mater. 61 (2013) 4354–4364.
[39] Z. Cui, F. Gao, J. Qu, Appl. Phys. Lett. 103 (2013).
[40] H. Yang, F. Fan, W. Liang, X. Guo, T. Zhu, S. Zhang, J. Mech. Phys. Solid. 70 (2014) 349–361.
[41] L. Luo, H. Yang, P. Yan, J.J. Travis, Y. Lee, N. Liu, D.M. Piper, S.H. Lee, P. Zhao, S. M. George, J.G. Zhang, Y. Cui, S. Zhang, C. Ban, C.M. Wang, ACS Nano 9 (2015) 5559–5566.
[42] Z. Jia, W.K. Liu, Appl. Phys. Lett. 109 (2016).
[43] K. Zhao, M. Pharr, Q. Wan, W.L. Wang, E. Kaxiras, J.J. Vlassak, Z. Suo, J. Electrochem. Soc. 159 (2012) A238–A243.
[44] M.T. Mcdowell, S.M. Xia, T. Zhu, Extreme Mechanics Letters 9 (2016) 480–494.
[45] Y. Huang, H. Yang, T. Xiong, D. Adekoya, W. Qiu, Z. Wang, S. Zhang, M.S. Balogun, Energy Storage Materials 25 (2020) 41–51.
[46] M.S. Balogun, H. Yang, Y. Luo, W. Qiu, Y. Huang, Z.Q. Liu, Y. Tong, Energy Environ. Sci. 11 (2018) 1859–1869.